Influence of El Niño Modoki on spring rainfall over south China

Juan Feng[1] and Jianping Li[1]

Received 7 October 2010; revised 30 March 2011; accepted 6 April 2011; published 7 July 2011.

[1] Using observed data sets from 1979 to 2006, the relationship between El Niño Modoki and spring rainfall over south China (SC) is investigated. Of particular interest is the difference in the influence on spring rainfall of typical El Niño events and the recently recognized El Niño Modoki events, which are characterized by distinct warm sea surface temperature anomalies (SSTA) in the central Pacific and weaker cold anomalies in the western and eastern parts of the basin. Associated with the SSTA, anomalous ascent occurs over the central Pacific and downward flow is observed over the eastern and western Pacific. The anomalous flow is associated with anomalous convergence in the upper troposphere over the western Pacific. SC is influenced by an anomalous anticyclonic circulation with prevailing northeasterly anomalies. The convective activity in SC becomes weaker, resulting in reduced rainfall. However, the situation is different in the case of El Niño, in terms of the influence on rainfall over SC. While El Niño Modoki events are accompanied by a significant reduction in rainfall over SC, there is enhanced rainfall associated with El Niño events. Moreover, there exists a strong asymmetry in the relationship between SC spring rainfall, typical El Niño–Southern Oscillation (ENSO) and ENSO Modoki events. It appears that these relationships are only statistically significant for positive events. The asymmetric influence of positive and negative in two ENSO phenomena may explain the difference in their respective relationships with spring rainfall over SC.

Citation: Feng, J., and J. Li (2011), Influence of El Niño Modoki on spring rainfall over south China, *J. Geophys. Res.*, *116*, D13102, doi:10.1029/2010JD015160.

1. Introduction

[2] El Niño–Southern Oscillation (ENSO) has a strong influence on rainfall over China. Previous studies have shown that during the decaying stage of ENSO, the following summer is characterized by positive rainfall anomalies over the Yangtze River valley and Huai-he River valley and negative anomalies over southern and northern China [e.g., *Huang and Wu*, 1989; *Zhang et al.*, 1999; *Feng and Hu*, 2004; *Xue and Liu*, 2008]. This relation can be demonstrated statistically, as the El Niño events in the boreal winter of 1982, 1986, and 1997 were associated with positive rainfall anomalies over the Yangtze and Huai-he River valleys, as well as negative rainfall anomalies over southern and northern China in the following summer. Recently, *Ding et al.* [2010] reported that since the late 1970s the influence of ENSO on the East Asian summer circulation has shown a significant strengthening, and the associated circulations have shown a southward shift [*Li et al.*, 2010]. This finding indicates that ENSO has a strong influence on rainfall variability in China, with this influence having become more pronounced in recent decades. However, during the El Niño event in winter of 1991, summer rainfall in 1992 was below average across the Yangtze River valley to the Huai-he River Basin. One possible explanation for this finding is an interevent difference in the pattern of El Niño sea surface temperature anomalies (SSTA). During the winter of 1991, the maximum SSTA was located over the International Dateline, instead of the eastern equatorial Pacific [*Trenberth and Stepaniak*, 2001].

[3] The leading mode of an empirical orthogonal function (EOF) analysis performed using tropical Pacific Ocean SST yields the well-known El Niño pattern, with peak SSTA in the eastern Pacific [e.g., *Rasmusson and Carpenter*, 1982; *Trenberth*, 1997; *Zhang et al.*, 2009]. The second mode of tropical Pacific Ocean variability is dependent on the study period. An EOF performed on tropical Pacific SSTA for time series longer than 50 years (i.e., 1880–2007 and 1948–2007) yielded a cooling mode in the equatorial Pacific cold tongue [*Zhang et al.*, 2010]. However, for the post-1970s period (i.e., 1979–2004), the second mode is represented by warm SSTA located in the central Pacific, accounting for approximately 12% of the total variance [*Ashok et al.*, 2007] (within 30°S–30°N). This mode corresponds to the third SST mode for long-term variability (i.e., 1880–2007 and 1948–2007) in the work of *Zhang et al.* [2010] over the tropical Pacific in the same domain. The mode, referred to as El Niño Modoki, is characterized by warm waters in the

[1]State Key Laboratory of Numerical Modeling for Atmospheric Sciences and Geophysical Fluid Dynamics, Institute of Atmospheric Physics, Chinese Academy of Sciences, Beijing, China.

0148-0227/11/2010JD015160

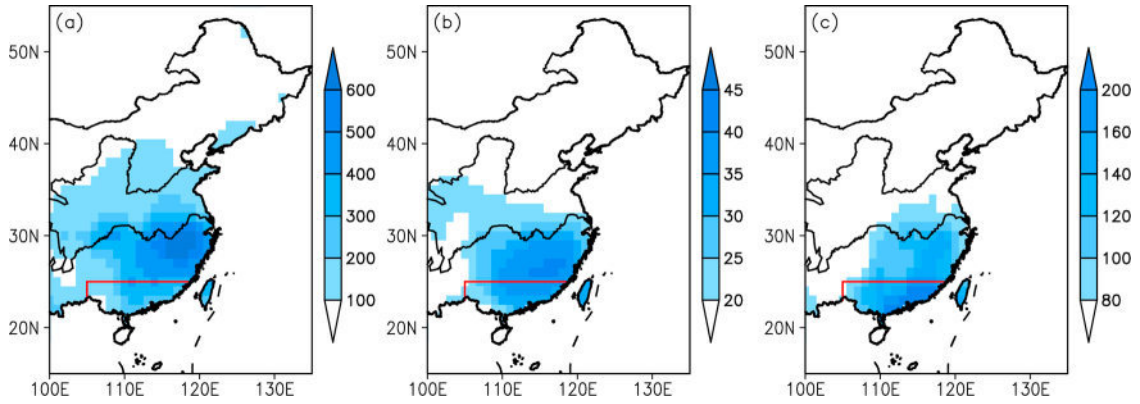

Figure 1. (a) Distribution of spring rainfall over China based on station data (unit: mm). (b) Percentage of the spring rainfall in the annual total (unit: %). (c) Standard deviation of the spring rainfall (unit: mm). South China is scaled in the red line.

central Pacific and cool waters in the eastern and western parts of the basin.

[4] *Ashok et al.* [2007] reported that El Niño Modoki is associated with a tripolar pattern of sea level pressure (SLP) anomalies during its evolution and documented the presence of two anomalous Walker circulation cells in the troposphere, instead of the single cell associated with the typical El Niño mode. The joint ascending branch of this double Walker circulation is located over the central equatorial Pacific, and the western descending branch is located over Indonesia and northern Australia. This configuration appears to influence regional climate in a different way to that of the typical El Niño. For example, *Weng et al.* [2007, 2009] analyzed three Modoki events with the aim of assessing their influence on climate over China, Japan, and the United States during the boreal summer (June–August) and winter (December–February). *Taschetto and England* [2009] examined the influence of El Niño Modoki on rainfall variability during the Australian autumn (March–May, MAM), revealing that MAM is the time of maximum rainfall anomalies induced by El Niño Modoki over Australia. *Cai and Cowan* [2009] investigated the influence of La Niña Modoki on Australian autumn (MAM) rainfall, showing that the difference between the influence of ENSO and ENSO Modoki (EM) on Australian rainfall is most conspicuous during MAM. W. J. Zhang et al. (Contrasting impacts of two-types El Niño over the western north Pacific during boreal autumn, submitted to *Journal of the Meteorology Society of Japan*, 2011) pointed out that the impacts of two types of ENSO exhibit contrasting differences in autumn rainfall over China.

[5] The above results indicate that the boreal spring (MAM) is an important season for EM, when the influence of EM on Australian rainfall is most pronounced. This period also generally corresponds to the first rainy season in south China (SC). Rainfall over SC in this season takes up as much as 30% of the annual total (Figure 1b). Further, the variance of spring rainfall over SC is most pronounced comparing to other regions over the eastern China during this season (Figure 1c). This point suggests that the spring rainfall over SC shows distinguishing characteristics and contributes a lot to the annual rainfall. In addition, spring rainfall has significant impacts on the agriculture. As SC has a large population and is an important economic region, rainfall variability has a strong influence on economic growth and the daily life of millions of people. The occurrence of flooding or drought in this region during MAM results in a large economic cost every year. Thus further studies on rainfall variation during this period, as well as its causes, would be important as both a scientific endeavor and in terms of disaster mitigation. In fact, previous studies have reported that variations in tropical Pacific SST have a strong influence on rainfall over SC during the first rainy season [e.g., *Cai et al.*, 2002; *Chen et al.*, 2003; *Chen and Qian*, 2005].

[6] The tropical Pacific SST mode-EM was recognized only recently; consequently, it remains unclear whether it has an influence on spring rainfall over SC. If such an influence exists, it would be important to consider the difference in the influences on rainfall of EM and typical ENSO events. Accordingly, one of the key goals of the present study is to extend the analysis of *Weng et al.* [2007, 2009] and to focus on the boreal spring (MAM), with the aim of further establishing the influence of EM on SC spring rainfall. The remainder of this manuscript is organized as follows. Section 2 describes the data sets and methods used in this study, and section 3 outlines the anomalies associated with EM and typical ENSO during MAM. Section 4 discusses the asymmetric relationship between SC spring rainfall and positive/negative phases of EM, and positive/negative phases of typical ENSO events. Finally, conclusions and discussions are provided in section 5.

2. Data and Methods

[7] Global SST is from the Improved Extended Reconstruction SST (IERSST) [*Smith and Reynolds*, 2004] on a 2° × 2° grid, and atmospheric fields are from the National Centers for Environmental Prediction–National Center for Atmospheric Research (NCEP/NCAR) reanalysis [*Kalnay et al.*, 1996]. Stream function data are from the European Centre for Medium–Range Weather Forecasts (ECWMF) reanalysis for the period 1958–2001 [*Uppala et al.*, 2005]. We employed monthly precipitation data from the CPC Merged Analysis of Precipitation (CMAP) [*Xie and Arkin*, 1997] and 160-station monthly mean rainfall data from the

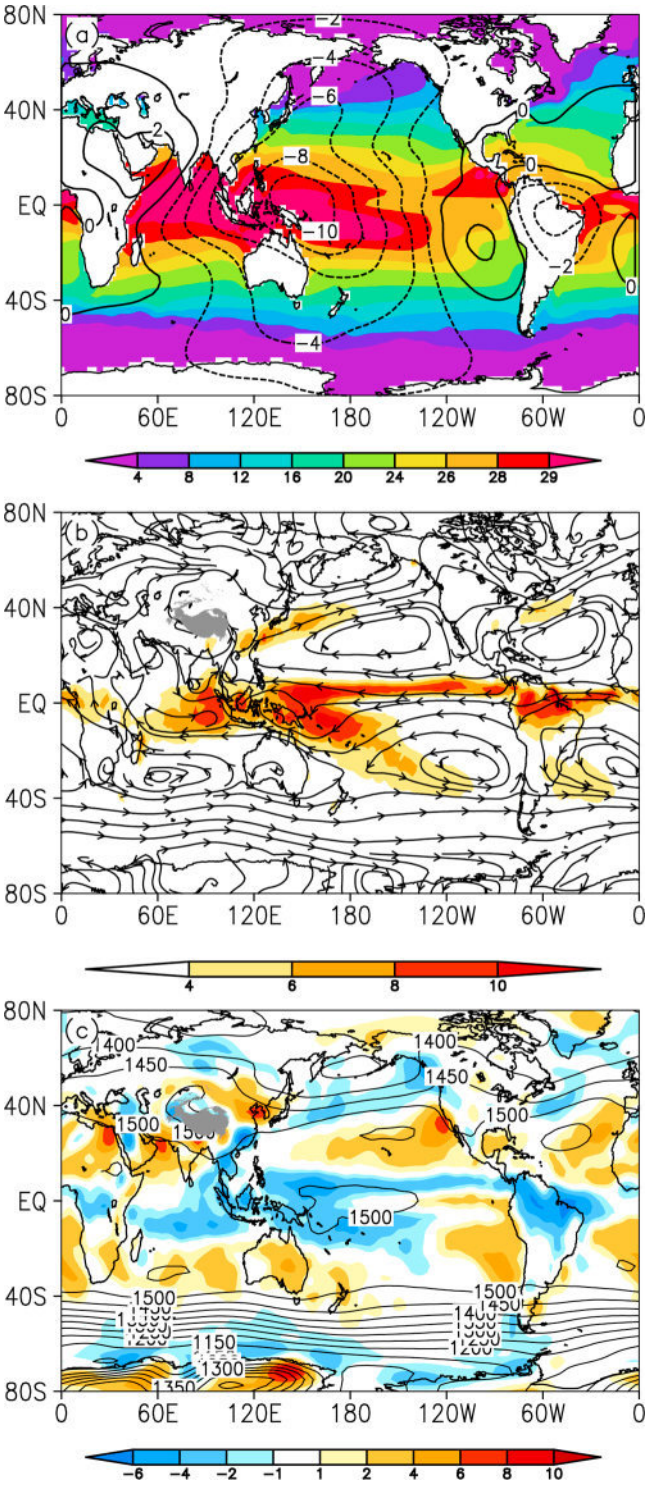

Figure 2. Boreal spring climatology for the period 1979–2006. (a) SST (shading, unit: °C) and velocity potential at 200 hPa (contours, interval: 2×10^6 m^{-2} s^{-1}). (b) CMAP precipitation rate (shading, unit: mm d^{-1}) and wind at 850 hPa (stream). (c) Geopotential height (contours, unit: gpm) at 850 hPa and vertical velocity at 500 hPa (shading, unit: 10^{-2} P s^{-1}).

Chinese Meteorology Administration (CMA). The outgoing long-wave radiation (OLR) monthly mean is from the National Oceanic and Atmospheric Administration (NOAA) [*Trenberth et al.*, 2002].

[8] Considering that EM has occurred mainly since the late 1970s and to avoid the modulation of Interdecadal Pacific Oscillation (IPO) [e.g., *Mantua et al.*, 1997; *Zhang et al.*, 1997], we focus on the boreal spring (March–May, MAM) during 1979–2006, which corresponds to the positive phase of IPO and a strengthened linkage between ENSO and East Asian circulation [*Ding et al.*, 2010]. Following *Ashok et al.* [2007], the ENSO Modoki index (EMI) is defined as

$$EMI = [SSTA]_c - 0.5 \times [SSTA]_E - 0.5 \times [SSTA]_w,$$

where square brackets with a subscript represent the areal mean SSTA over the central Pacific region (C: 165°E–140°W, 10°S–10°N), eastern Pacific region (E: 110°–70°W, 15°S–5°N), and western Pacific region (W: 125°–145°E, 10°S–20°N). These regions are marked in Figure 5a. The canonical ENSO is quantified by the Niño3 index, which is defined as the areal mean SSTA over the region (150°–90°W, 5°S–5°N) and is available online (http://www.cpc.noaa.gov/data/indices/).

[9] Singular value decomposition (SVD) analysis can be used to determine two coupled sets of orthogonal singular vectors, as well as the expansion coefficient correlations from the covariance matrix of two geophysical fields [*Wallace et al.*, 1992; *Cherry*, 1996]. Here, SVD analysis is used to reveal the coupled spatial patterns between SSTA in the tropical Pacific and rainfall anomalies over China. Correlation and composite analyses are employed to investigate the relationship between EM and spring rainfall over China. In addition, partial correlation [*Ashok et al.*, 2003; *Weng et al.*, 2007; *Feng et al.*, 2010], which is commonly used to calculate the correlation between two variables after removing the effects of another variable, is employed to examine the relationship between EM or ENSO and SC rainfall.

3. Anomalies of Canonical ENSO and EM

3.1. Climatological Mean

[10] The normal spring climate fields are given in Figure 2 as a reference to show the background setting and to reveal differences between ENSO and EM years. Figure 2a shows the normal SST distribution. The warmest SST is located in the warm pool of the western Pacific near New Guinea, south of the equator. A secondary warm center is located in the eastern Pacific "cold tongue" and tropical Atlantic. Accordingly, the main center of divergence at upper levels (200 hPa) in the troposphere is over the western Pacific, extending to the central Pacific near 130°W. SC is influenced by a divergence at upper levels. The distribution of the velocity potential in the lower troposphere is opposite to that in the upper troposphere (figures not shown), in which the divergence center is replaced by a convergence center with a slight northwestward shift. Associated with the upper level divergence, strong upward flow occurs over the warm pool, SC, and northern South America (Figure 2c). The subtropical highs in both hemispheres are centered at a

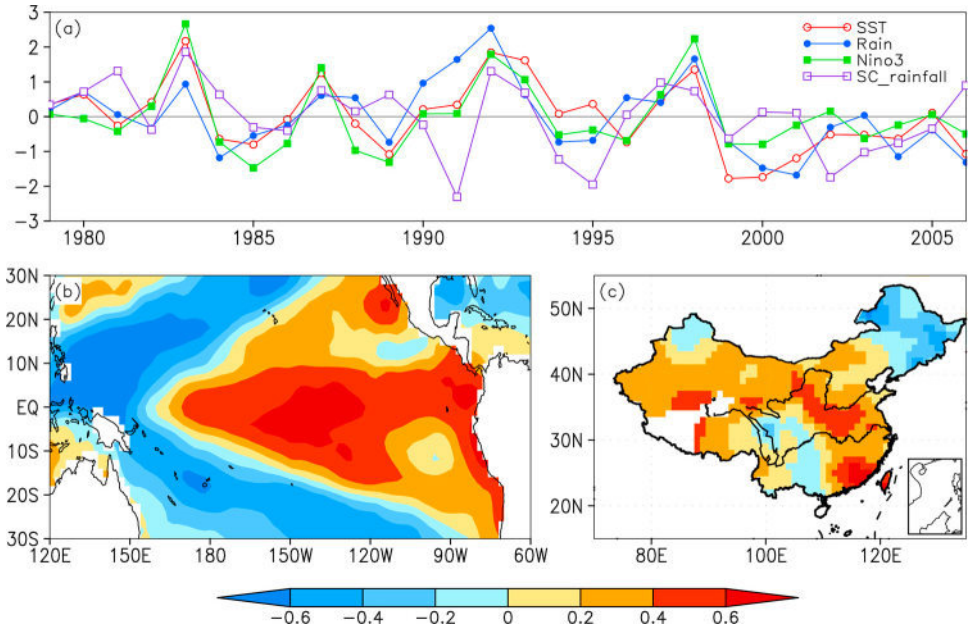

Figure 3. (a) The normalized expansion coefficients of anomalous spring tropical Pacific SST and rainfall for the first dominant coupled mode of the SVD. Also shown are the normalized time series of Niño 3 index and south China rainfall during spring. Red line: expansion coefficient of the SSTA mode; blue line: expansion coefficient of the anomalous rainfall mode; green line: Niño3 index; purple line: south China spring rainfall. (b) The heterogeneous correlation pattern for the first dominant coupled mode for the spring SSTA. (c) Same as Figure 3b but for the spring rainfall in China.

latitude of about 30°, separated by continents in areas of downward flow (Figure 2b). The Aleutian low over the northern Pacific is apparent in both circulation and geopotential height fields, with a corresponding rising flow over the northern Pacific. Along with the distribution of divergence (Figure 2a), vertical velocity (Figure 2c), and horizontal circulation (Figure 2b), the main rainband is located over the warm pool, eastern Indian Ocean, along the intertropical convergence zone in the Pacific and Atlantic, along the south Pacific convergence zone, and northern South America.

[11] The distributions of Walker circulation (averaged over 10°S to 10°N) and velocity potential (figures not shown) indicate that the rainfall distribution in Figure 2b is well connected to Walker circulation over the tropical Pacific, with the main upward flow occurring from 90°E to 150°W. Figure 1a shows the average distribution of spring rainfall in China, revealing contrasting rainfall amounts between northern China (relatively minor rainfall) and SC (heavy rainfall in the area east of 105°E and south of 25°N). These data provide further evidence of the importance of variations in spring rainfall over SC.

3.2. SVD Analysis

[12] SVD analysis was performed on the normalized time series during MAM of tropical Pacific SST and rainfall over China. The first coupled mode of tropical Pacific SST corresponds to the ENSO pattern (Figure 3b), as the correlation coefficient between the time series of SVD expansion coefficients and the Niño3 index is 0.85 (Figure 3a). This corresponds to positive SSTA over the eastern Pacific and negative anomalies over the western Pacific. This pattern is accompanied by positive rainfall anomalies over most of eastern China, except northeastern areas (Figure 3c). The strong coupling between ENSO and rainfall over China is responsible for 58% of the squared covariance fraction. The associated time series of SST and rainfall yield a correlation coefficient of 0.76, significant at the 0.05 level.

[13] The second coupled mode of SST is related to the EM pattern (Figure 4), with warm SST in the Pacific and cool SST in the western and eastern Pacific. This mode accounts for 11% of the squared covariance fraction. This coupling between the SST and rainfall mode is indicated by a significant correlation coefficient of 0.76 at the 0.01 level between the time series of expansion coefficients of both variables and is associated with contrasting rainfall anomalies over China. In contrast to most of eastern China, which shows similar features to the ENSO-induced pattern, SC is characterized by negative rainfall anomalies. The time series of expansion coefficients for SST is strongly correlated with EMI (correlation coefficient = 0.71).

[14] The above analysis reveals that EM has a strong influence on spring rainfall over China. The influence of EM is the opposite to that of typical ENSO, particularly for SC.

3.3. Associated Circulation Anomalies

[15] To access the robustness of the SVD analysis, we also considered the partial correlation between EM/ENSO and SST, after removing the effects of ENSO/EM as appropriate. The correlation pattern with EM shows significant positive correlations over the central tropical Pacific

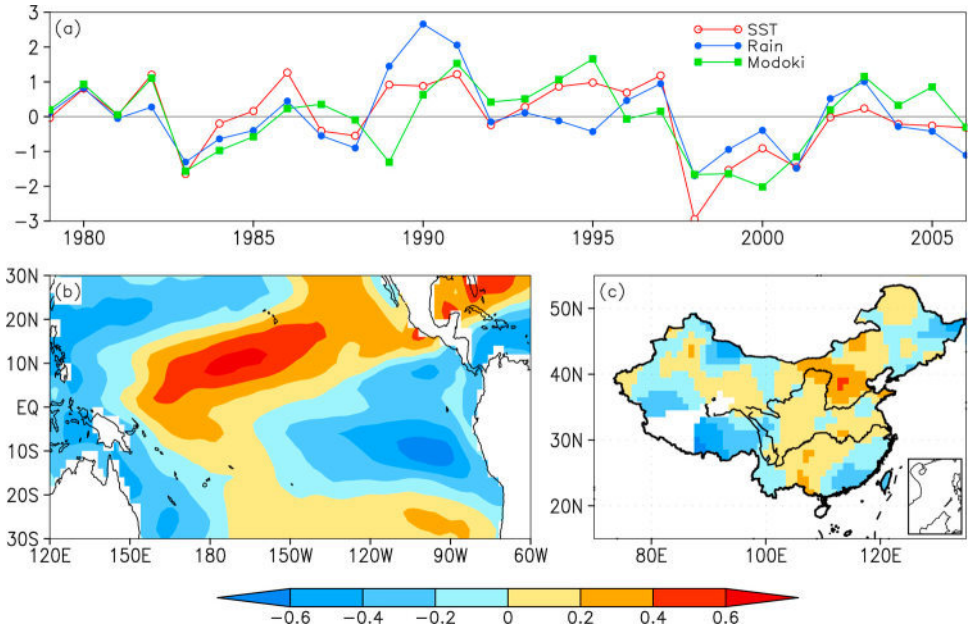

Figure 4. Same as Figure 3 but for the second dominant coupled mode. Also shown is the normalized time series of spring ENSO Modoki index.

and negative correlations over the western and eastern Pacific (Figure 5a). Accordingly, anomalous divergence occurs in the central tropical Pacific and in association with convergence over the western and eastern Pacific in the upper troposphere (200 hPa); however, the opposite pattern is seen in the lower troposphere (figures not shown).

[16] The anomalous pattern associated with ENSO in MAM shows significant positive SSTA in the eastern Pacific (Figure 5b). In response to this SSTA pattern, divergence occurs at high levels in the troposphere over the eastern Pacific (figures not shown). The western Pacific shows negative SSTA associated with divergence in the lower troposphere. Note that the result here is similar to that in the work of *Ashok et al.* [2003] although there are different seasons focused. Similar negative SSTA is seen over the western Pacific for both EM and ENSO, but the SSTA associated with ENSO are located southeast of those in the case of EM and are larger and stronger. Moreover, positive SSTA occur in the East Asian marginal seas and Indian Ocean in the case of ENSO [*Wang et al.*, 2000], whereas nonsignificant signal is seen in the EM situation. These results indicate that the EM and ENSO cases differ not only in the locations of the warming centers around the equator but also in the related SSTA over the East Asian marginal seas and the Indian Ocean.

[17] Figure 6 shows circulation anomalies associated with EM and ENSO for horizontal circulation patterns in the lower troposphere. Under the influence of basin-wide warming over the central Pacific during EM, negative geopotential height anomalies occur over the central Pacific, centered at 20°N, 160°W (Figure 6c). Simultaneously, cooling over the western Pacific induces positive anomalies in geopotential height, South China Sea (SCS), and Kuroshio extension, indicating anomalous anticyclonic circulation over these regions. Against this background, anomalous downward flow

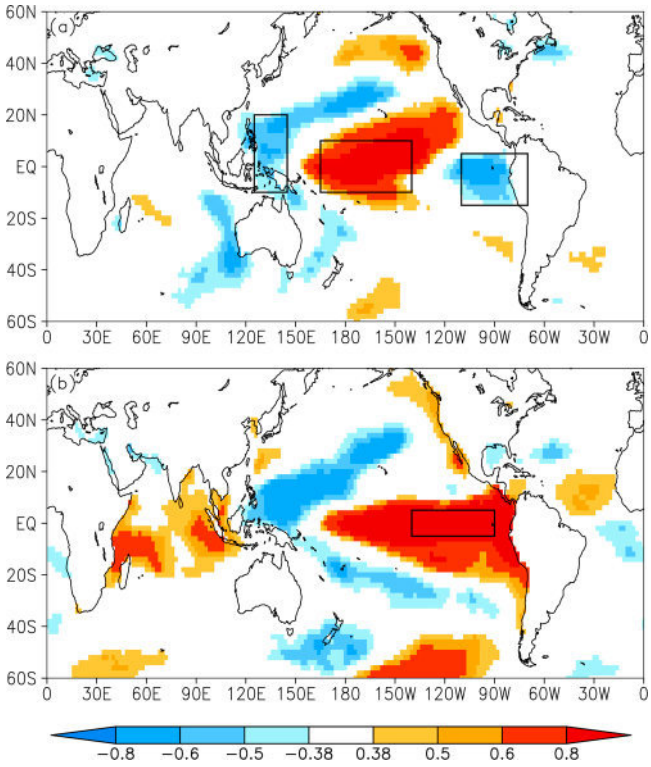

Figure 5. (a) Partial correlation between EMI and SST during MAM from 1979 to 2006, after removing the effects of ENSO. (b) Same as Figure 5a but between the Niño3 index and SST, after removing the effects of ENSO Modoki. The black rectangles indicate the areas used to calculate the respective indices. Color shading indicates a significant correlation at the 0.05 level (0.38 is the critical value for significance at the 0.05 level).

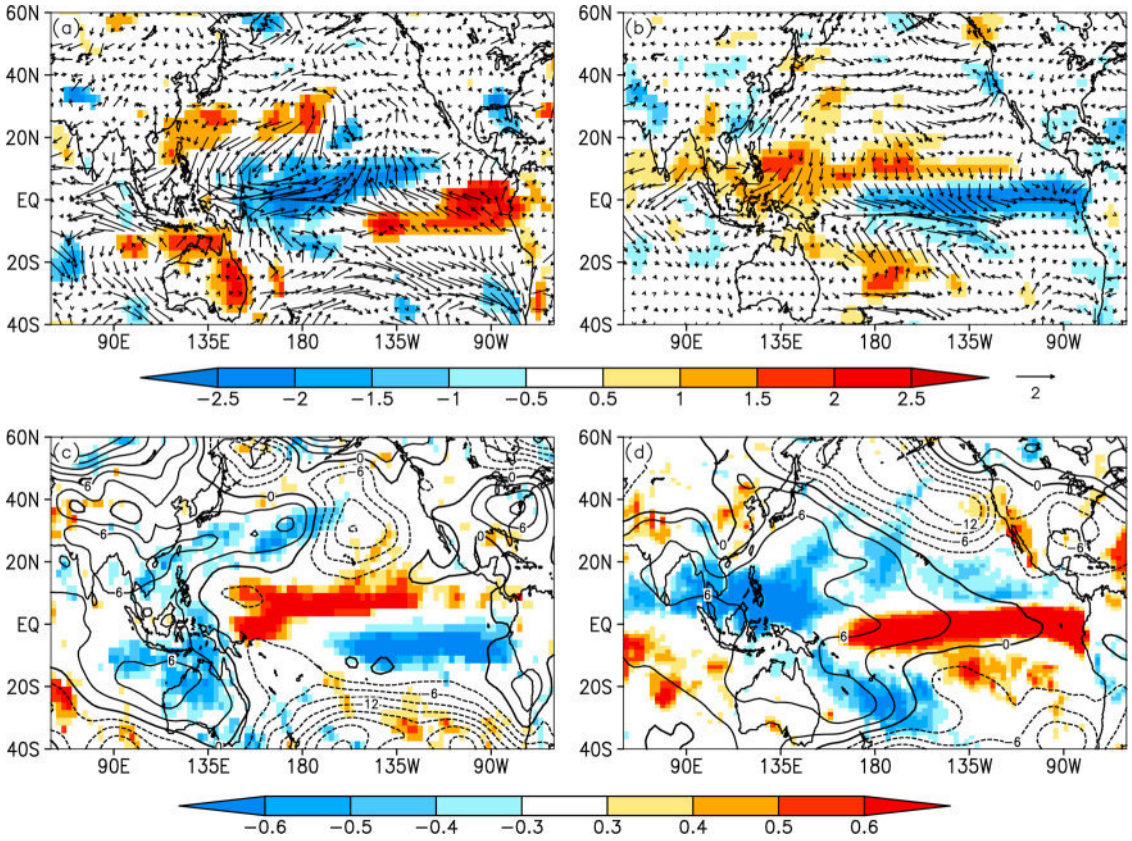

Figure 6. Regression anomalous patterns of surface wind (vectors) with respect to (a) EMI and (b) Niño 3 index; shading indicates vertical velocity that is statistically significant at the 0.1 level. (c and d) Same as Figures 6a and 6b, respectively, but for the regression patterns with geopotential height (at 850 hPa, contours); shading indicates correlations with the rainfall.

and northeasterlies prevail over SC (Figure 6a), indicating weaker than normal southwesterlies over SC, resulting in reduced rainfall (Figure 6c).

[18] For the ENSO case, the equatorial eastern Pacific warming induces a cyclonic response to the northwest (for the Northern Hemisphere (NH), centered about 35°N, 140°W) or southwest (for the Southern Hemisphere (SH), centered about 20°S, 130°W) of the warming (Figure 6b). This response is manifested by equatorward flow associated with the equatorial westerly anomalies over the eastern Pacific (Figure 6b). In the western Pacific, since the cooling center is south of that in the case of EM, the anomalous anticyclone center is also located to the south. Consequently, SC is located to the rear of the anomalous western Pacific anticyclone, suggesting that anomalous southwesterlies prevail in the region (Figure 6b), in turn indicating stronger than normal southwesterlies over SC. Anomalous upward flow occurs over SC due to warming along the coast. The combination of anomalous southwesterlies and rising flow results in a wet spring in SC (Figure 6d).

4. Asymmetry of EM and ENSO

[19] The above analysis suggests that EM and ENSO have opposite effects on spring (MAM) rainfall over SC, with EM having a negative influence and ENSO having a positive influence. Focusing on SC, we find that EMI and the Niño3 index are significantly correlated with temporal variations in rainfall (correlation coefficients of −0.49 and 0.41, respectively; Figure 3a). To further investigate their influences on spring rainfall over SC, Figure 7 shows the relation between spring rainfall in SC and each of EMI and the Niño3 index. El Niño Modoki and La Niña Modoki have an asymmetric influence, as do El Niño and La Niña. For positive values of the indices, the correlation coefficients between rainfall, and EMI and Niño3 index are −0.64 and 0.74, respectively, both exceeding the 0.01 level of significance. In contrast, for negative phases of EM and ENSO, the influence on rainfall is not statistically significant, yielding correlation coefficients of −0.14 and −0.05 for EMI and Niño3 index, respectively. Thus typical ENSO affects spring rainfall in SC, but the influence is only statically significant during its positive phase. Similarly, the influence of EM on spring rainfall in SC is only apparent during El Niño Modoki.

[20] The asymmetric influences of ENSO and EM on spring rainfall in SC are also apparent in the horizontal distribution of correlation coefficients (Figure 8). During the events of El Niño Modoki/El Niño, statistically significant negative/positive correlations are seen over SC, whereas a nonsignificant signal is found in this region for La Niña

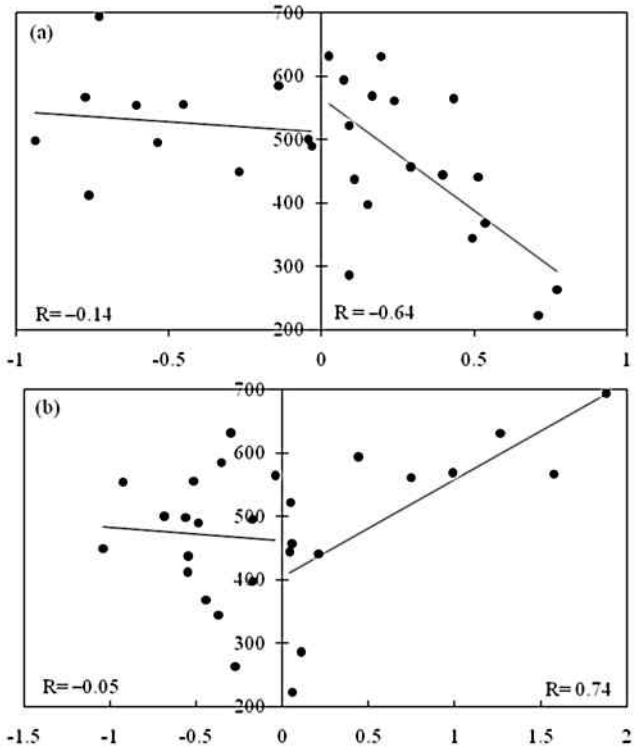

Figure 7. Spring rainfall in SC plotted against (a) EMI and (b) Niño3 index. Also shown are lines of best fit for positive and negative EMI/Niño3 index values and correlation coefficients.

Modoki/La Niña. This result suggests that the significant relationships between EM/ENSO and spring rainfall over SC are associated mainly with positive events. Furthermore, El Niño Modoki and typical El Niño events are associated with the opposite rainfall anomalies in SC; thus the corresponding reversed anomalies of EM and ENSO are derived mainly from the contrasting effects of El Niño Modoki and El Niño events.

[21] Figure 9 shows the anomalous patterns for lower troposphere wind, geopotential height at 850 hPa, and OLR during the five strongest positive events for both EM (1982, 1991, 1994, 1995, and 2003) and ENSO (1983, 1987, 1992, 1993, and 1998). The anomalous circulation patterns in Figure 9 are similar to those in Figure 6. In response to basin warming over the central Pacific, negative geopotential height anomalies form over the central Pacific (Figure 9c). The anomalous negative centers in the NH contain two distinct centers, at 10°N, 150°E and 20°N, 130°W, suggesting the cyclonic anomaly in the NH is oriented northeast-southwest (NE-SW). The anomalies in geopotential height are accompanied by cyclonic rotation (Figure 9e) and anomalous northeasterlies over the western Pacific (Figure 9a), indicating that the prevailing wind is weakened in this region, associated with negative SSTA oriented NE-SW. Since the cooling over the western Pacific is oriented NE-SW, with the largest values at around 30°N, 180°E (Figure 5a), anticyclonic rotational flow occurs over these regions with two centers: 40°N, 180°E and directly over SC (Figure 9e). This result indicates that the position of the western Pacific subtropical high (WPSH) is shifted northward (as also observed from the location of the WPSH; figures not

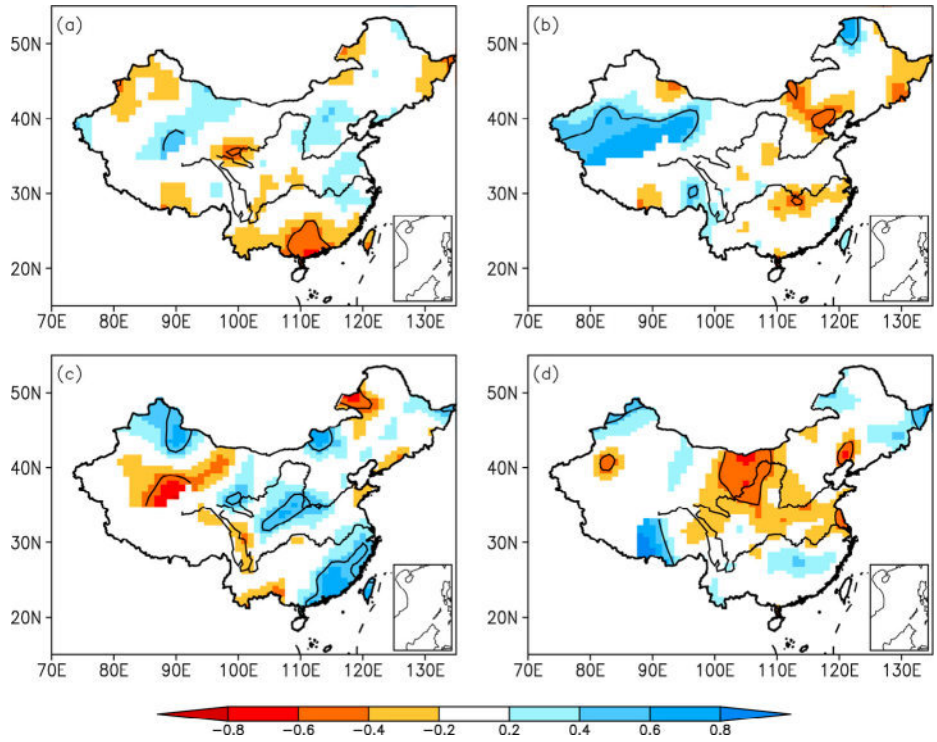

Figure 8. Spatial distribution of correlation coefficients between (a) positive and (b) negative EMI values and spring rainfall from 1979 to 2006. (c and d) Same as Figures 8a and 8b, respectively, but for the Niño3 index. Areas with black contours are statistically significant at the 0.1 level.

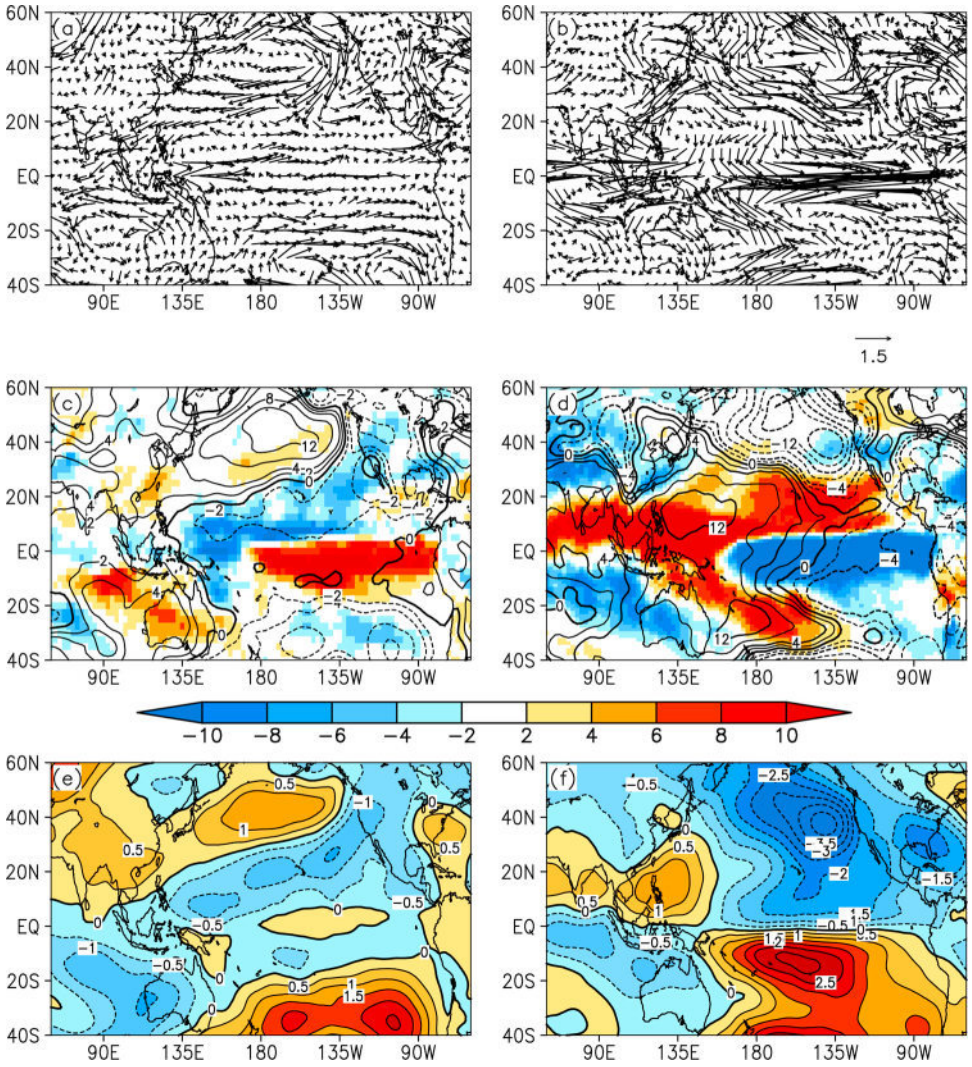

Figure 9. Anomalous patterns during the El Niño Modoki years for (a) wind (vectors, unit: m/s), (c) geopotential height (contours, unit: gpm) at 850 hPa, OLR (shading, unit: W m^{-2}), and (e) stream function at 850 hPa (unit: 10^6 m^{-2} s^{-1}). (b, d, and f) Same as Figures 9a, 9c, and 9e, respectively, but for the El Niño years. In Figure 9e, four El Niño Modoki events (1982, 1991, 1994, and 1995) are included since the limitation of length for the ECMWF data; the rest is the composite of five events (El Niño Modoki: 1982, 1991, 1994, 1995, and 2003; El Niño: 1983, 1987, 1992, 1993, and 1998).

shown). In this setting, SC is affected by anomalous northeasterlies (Figure 9a) that are the reverse to the normal circulation, thus moist transportation to SC by southwesterlies is reduced, resulting in suppressed rainfall, which is further manifested by weakened convective activity over SC (Figure 9c).

[22] During El Niño events, warming in the eastern Pacific results in asymmetric cyclonic anomalies (Figure 9f) at either side of equator, with strong equatorial westerly anomalies (Figure 9b). The anomalous westerlies indicate that the trade wind is weakened, associated with a negative SSTA in the western Pacific [*Wang et al.*, 2000]. Under the influence of this cooling, asymmetric stream function anomalies are located in each hemisphere, indicating anticyclonic rotational flow. The anticyclonic anomaly over the western Pacific in the NH is centered at 15°N, 135°E, indicating a southward shift of the WPSH (Figures 9b and 9f) which is similar to that in the work of *Wang et al.* [2000] despite different seasons referred, corresponding to anomalous southwesterlies over SCS and SC (Figure 9b). Consequently, the combination of anomalous cyclonic rotation and a southeastward shift of WPSH results in southwesterly anomalies over SC, which strengthen the moist transport to this region and favor enhanced rainfall. This scenario is verified by the anomalous distribution of OLR because convective activity over SC is strengthened during El Niño events (Figure 9d).

[23] Here, we highlight several strong spring seasons with values of rainfall above/below 1 standard deviation from the average value for the period 1979–2006 (Figure 10). Four of the five driest springs are connected to paralleling records in El Niño Modoki, and two of the three wettest springs

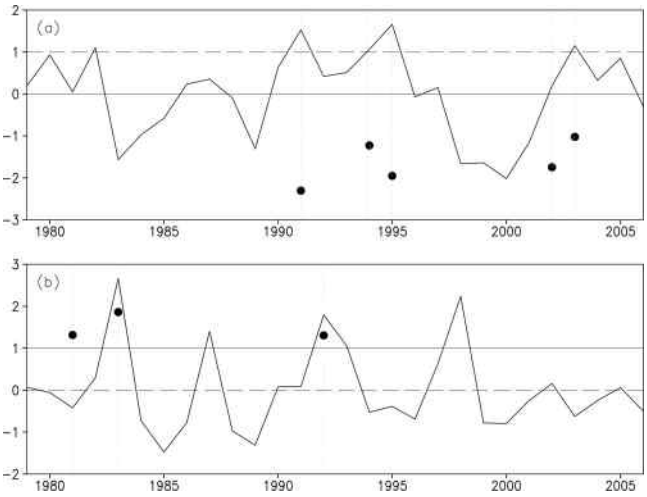

Figure 10. Normalized time series (1979–2006) of (a) EMI and (b) Niño3 index, showing the five driest and three wettest springs in SC (black dots). The horizontal dashed lines indicate 1 standard deviation from the average value.

are coincident with well-defined El Niño events. The best examples of the asymmetric influences of ENSO and ENSO Modoki are seen for the spring seasons in 1985 and 1989, during La Niña events. Because the relationship only exists in El Niño events, these periods are associated with normal rainfall in SC. The spring seasons in 1999 and 2000, during La Niña Modoki years, also show normal rainfall (Figure 3a). The rainfall during spring in 1991 (a clear El Niño Modoki year) was the lowest during the period 1979–2006 because Modoki has a negative influence on spring rainfall in SC. In addition, the spring seasons in 1994 and 1995 were two of the five driest years during the period 1979–2006, corresponding to well-defined El Niño Modoki events. Spring in 1992 was associated with abundant rainfall over SC, during an El Niño event. In addition, spring in 1983 was an El Niño year, combined with a La Niña Modoki event, resulting in the wettest spring in SC during period 1979–2006. These results demonstrate that although spring rainfall in SC is influenced by both ENSO and EM, they only manifest during positive events.

5. Conclusions and Discussions

[24] Using recent 28-year observational data sets, we demonstrated that spring rainfall in SC is influenced by both typical ENSO and the newly recognized ENSO Modoki. Both are primary factors in controlling tropical Pacific SST, which affects spring rainfall in SC. The different circulation anomalies of these events are associated with the opposite rainfall anomalies in SC, i.e., El Niño Modoki is accompanied by reduced rainfall, and El Niño events are characterized by enhanced rainfall.

[25] Figure 11 shows a schematic of the processes that potentially explain the influence of El Niño Modoki and El Niño on spring rainfall in SC. For El Niño Modoki years, anticyclonic anomalies occur over SC, indicating that SC is influenced by anticyclonic rotation with prevailing anomalous northeasterlies; this setting is the reverse to the normal circulation and results in suppressed rainfall over this region (Figure 11a). For El Niño years, in contrast, cyclonic rotation is observed along with an anomalous anticyclone over the western Pacific centered at 15°N, 135°E, indicating a southeastward shift in the WPSH (Figure 11b). Consequently, SC is affected by anomalous southwesterlies that result in enhanced spring rainfall. Note that the scheme associated with ENSO is similar to that in the work of *Wang et al.* [2000]; however, the present study focuses on the boreal spring rather than winter, and we consider SC in terms of differences in inter-event difference between El Niño Modoki and El Niño.

[26] There exists an asymmetry between the influences on rainfall in SC of El Niño Modoki and La Niña Modoki events. El Niño Modoki events have a statistically significant influence on SC spring rainfall but not in the La Niña Modoki events. This situation is also observed for the relationship between Niño3 index and SC spring rainfall (i.e., only El Niño events have a significant influence on SC spring rainfall). This asymmetry (i.e., that El Niño Modoki is linked with negative rainfall anomalies in SC) provides a plausible explanation for strong inter-ENSO variations in spring rainfall observed over SC. This includes the spring of 1991, when rainfall was the lowest during the period 1979–2006, corresponding to a well-recorded El Niño Modoki event. In addition, the spring seasons in 1985 and 1989, which occurred during well-defined La Niña events, had normal rainfall in SC. The contrasting influences of positive and negative EM/ENSO may explain the corresponding relationship between ENSO and variations in SC spring rainfall.

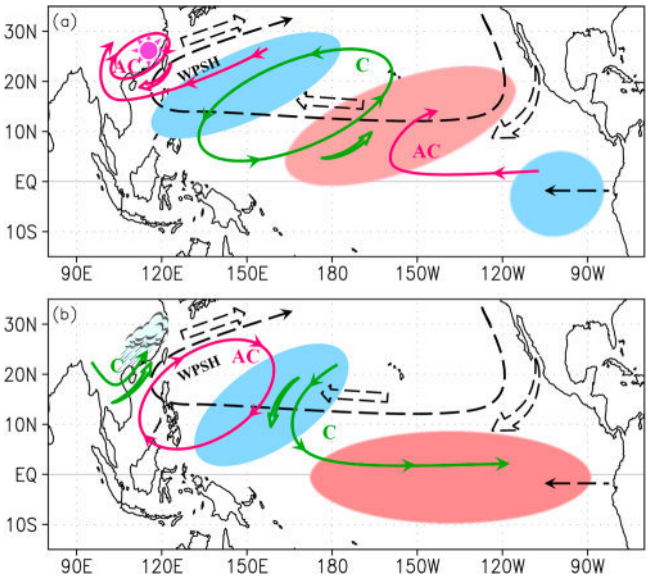

Figure 11. Schematic diagrams showing the circulation anomalies associated with (a) El Niño Modoki and (b) El Niño. Red/blue shaded areas indicate positive/negative SSTA. WPSH: western Pacific subtropical high. Dashed lines represent the climatological mean. Solid lines indicate anomalous circulation, and heavy arrows represent anomalous wind directions. "C" and "AC" indicate cyclonic and anticyclonic circulation anomalies, respectively.

[27] Independent of this work, a recent study of *Cai et al.* [2010] showed an asymmetry in the relationship between rainfall over northeast Australia and ENSO phases and attributed this to the multidecadal variability associated with the IPO. The relationships between the EM/ENSO and SC spring rainfall are further checked for the period prior to 1979 (i.e., 1951–1978). We find that the asymmetry relationship between the EM/ENSO and SC spring rainfall are not hold (figures not shown), seeming that the relationship between the EM/ENSO and SC spring rainfall undergoes a multidecadal variation. Thus what is the possible reason, whether IPO plays any roles in modulating their relationships? Future work is required to determine what is the potential contributor of the multidecadal variation in their relationships?

[28] Finally, the present results highlight the fact that EM and ENSO have opposite climatic influences on spring rainfall in SC, and there exists an asymmetry between positive and negative values in both ENSO phenomena during period 1979–2006. These findings underscore the importance of taking into account the influence of El Niño Modoki on spring rainfall over SC when studying the influence of ENSO. Furthermore, the impacts of ENSO on Chinese climate have been extensive explored, whether does the asymmetric relationship between positive and negative events also exist in other seasons in terms of the ENSO/EM–rainfall relationship warranty more work.

[29] **Acknowledgments.** We thank two anonymous referees, whose comments improved the paper. This work was jointly supported by the 973 Program (2010CB950400) and the National Natural Science Foundation of China (41030961) and CAS Project (XDA5090403).

References

Ashok, K., Z. Y. Guan, and T. Yamagata (2003), Influence of the Indian Ocean dipole on the Australian winter rainfall, *Geophys. Res. Lett.*, *30*(15), 1821, doi:10.1029/2003GL017926.

Ashok, K., et al. (2007), El Niño Modoki and its teleconnection, *J. Geophys. Res.*, *112*, C11007, doi:10.1029/2006JC003798.

Cai, W. J., and T. Cowan (2009), La Niña Modoki impacts Australia autumn rainfall variability, *Geophys. Res. Lett.*, *36*, L12805, doi:10.1029/2009GL037885.

Cai, X. Z., Y. Wang, and J. J. Xu (2002), Diagnostic analysis on impact of convective activity anomalies over tropic on flood, drought during the first rainy season in south China (in Chinese), *J. Trop. Meteorol.*, *18*(2), 158–161.

Cai, W. J., P. Rensch, T. Cowan, and A. Sullivan (2010), Asymmetry in ENSO teleconnection with regional rainfall, its multidecadal variability, and impact, *J. Clim.*, *23*, 4944–4955, doi:10.1175/2010JCLI3501.1.

Chen, Y. M., and Y. F. Qian (2005), Numerical study of influence of the SSTA in western Pacific warm pool on precipitation in the first flood period in south China (in Chinese), *J. Trop. Meteorol.*, *21*(1), 13–23.

Chen, S. D., Q. Q. Wang, and Y. F. Qian (2003), Preliminary discussions of basic climatic characteristics of precipitation during raining seasons in regions south of Changjiang River and its relationship with SST anomalies (in Chinese), *J. Trop. Meteorol.*, *19*(3), 260–268.

Cherry, S. (1996), Singular value decomposition analysis and canonical correlation analysis, *J. Clim.*, *9*, 2003–2009, doi:10.1175/1520-0442(1996)009<2003:SVDAAC>2.0.CO;2.

Ding, R. Q., K. Ha, and J. P. Li (2010), Interdecadal shift in the relationship between the East Asian summer monsoon and the tropical Indian Ocean, *Clim. Dyn.*, *34*, 1059–1071, doi:10.1007/s00382-009-0555-2.

Feng, S., and Q. Hu (2004), Variations in the teleconnection of ENSO and summer rainfall in northern China: A role of the Indian summer monsoon, *J. Clim.*, *17*, 4871–4881, doi:10.1175/JCLI-3245.1.

Feng, J., J. P. Li, and Y. Li (2010), A monsoon-like southwest Australian circulation and its relation with rainfall in southwest Western Australia, *J. Clim.*, *23*, 1334–1353, doi:10.1175/2009JCLI2837.1.

Huang, R. H., and Y. F. Wu (1989), The influence of ENSO on the summer climate change in China and its mechanism, *Adv. Atmos. Sci.*, *6*(1), 21–32, doi:10.1007/BF02656915.

Kalnay, E., et al. (1996), The NCEP/NCAR reanalysis project, *Bull. Am. Meteorol. Soc.*, *77*, 437–471, doi:10.1175/1520-0477(1996)077<0437:TNYRP>2.0.CO;2.

Li, J. P., et al. (2010), Can global warming strengthen the East Asian summer monsoon?, *J. Clim.*, *23*, 6696–6705, doi:10.1175/2010JCLI3434.1.

Mantua, N. J., et al. (1997), A Pacific interdecadal climate oscillation with impacts on salmon production, *Bull. Am. Meteorol. Soc.*, *78*, 1069–1079, doi:10.1175/1520-0477(1997)078<1069:APICOW>2.0.CO;2.

Rasmusson, E. M., and T. H. Carpenter (1982), Variations in tropical sea surface temperature and surface wind fields associated with the Southern Oscillation/El Niño, *Mon. Weather Rev.*, *110*, 354–384, doi:10.1175/1520-0493(1982)110<0354:VITSST>2.0.CO;2.

Smith, T. M., and R. W. Reynolds (2004), Improved extended reconstruction of SST (1854–1997), *J. Clim.*, *17*, 2466–2477, doi:10.1175/1520-0442(2004)017<2466:IEROS>2.0.CO;2.

Taschetto, A. S., and M. H. England (2009), El Niño Modoki impacts on Australian rainfall, *J. Clim.*, *22*, 3167–3174, doi:10.1175/2008JCLI2589.1.

Trenberth, K. E. (1997), The definition of El Niño, *Bull. Am. Meteorol. Soc.*, *78*, 2771–2777, doi:10.1175/1520-0477(1997)078<2771:TDOENO>2.0.CO;2.

Trenberth, K. E., and D. P. Stepaniak (2001), Indices of El Niño evolution, *J. Clim.*, *14*, 1697–1701, doi:10.1175/1520-0442(2001)014<1697:LIOENO>2.0.CO;2.

Trenberth, K. E., D. P. Stepaniak, and J. M. Caron (2002), Interannual variations in the atmospheric heat budget, *J. Geophys. Res.*, *107*(D8), 4066, doi:10.1029/2000JD000297.

Uppala, S. M., et al. (2005), The ERA–40 re-analysis, *Q. J. R. Meteorol. Soc.*, *131*, 2961–3012, doi:10.1256/qj.04.176.

Wallace, J. M., C. Smith, and C. S. Bretherton (1992), Singular value decomposition of wintertime sea surface temperature and 500-mb height anomalies, *J. Clim.*, *5*, 561–576, doi:10.1175/1520-0442(1992)005<0561:SVDOWS>2.0.CO;2.

Wang, B., R. G. Wu, and X. H. Fu (2000), Pacific–East Asian teleconnection: How does ENSO affect East Asian Climate?, *J. Clim.*, *13*, 1517–1536, doi:10.1175/1520-0442(2000)013<1517:PEATHD>2.0.CO;2.

Weng, H. Y., et al. (2007), Impacts of recent El Niño Modoki on dry/wet conditions in the Pacific rim during boreal summer, *Clim. Dyn.*, *29*, 113–129, doi:10.1007/s00382-007-0234-0.

Weng, H. Y., S. K. Behera, and T. Yamagata (2009), Anomalous winter climate conditions in the Pacific rim during recent El Niño Modoki and El Niño events, *Clim. Dyn.*, *32*, 663–674, doi:10.1007/s00382-008-0394-6.

Xie, P. P., and P. A. Arkin (1997), Global precipitation: A 17-year monthly analysis based on gauge observations, satellite estimates, and numerical model outputs, *Bull. Am. Meteorol. Soc.*, *78*, 2539–2558, doi:10.1175/1520-0477(1997)078<2539:GPAYMA>2.0.CO;2.

Xue, F., and C. Z. Liu (2008), The influence of moderate ENSO on summer rainfall in eastern China and its comparison with strong ENSO (in Chinese), *Chin. Sci. Bull.*, *53*(5), 791–800, doi:10.1007/s11434-008-0002-5.

Zhang, Y., J. M. Wallace, and D. S. Battisti (1997), ENSO-like interdecadal variability: 1900–93, *J. Clim.*, *10*, 1004–1020, doi:10.1175/1520-0442(1997)010<1004:ELIV>2.0.CO;2.

Zhang, R. H., A. Sumi, and M. Kimoto (1999), A diagnostic study of the impact of El Niño on the precipitation in China, *Adv. Atmos. Sci.*, *16*(2), 229–241, doi:10.1007/BF02973084.

Zhang, W. J., J. P. Li, and F. F. Jin (2009), Spatial and temporal features of ENSO meridional scales, *Geophys. Res. Lett.*, *36*, L15605, doi:10.1029/2009GL038672.

Zhang, W. J., J. P. Li, and X. Zhao (2010), Sea surface temperature cooling mode in the Pacific cold tongue, *J. Geophys. Res.*, *115*, C12042, doi:10.1029/2010JC006501.

J. Feng and J. Li, State Key Laboratory of Numerical Modeling for Atmospheric Sciences and Geophysical Fluid Dynamics, Institute of Atmospheric Physics, Chinese Academy of Sciences, Beijing 100029, China. (ljp@lasg.iap.ac.cn)